

Pushing the Limits of Distillation-Based Class-Incremental Learning via Lightweight Plugins

Zhiming Xu^{1,2}, Baile Xu^{1,2}, Jian Zhao³, Furao Shen^{1,2}, Suorong Yang^{1,3,†}

¹ National Key Laboratory for Novel Software Technology, Nanjing University, China

² School of Artificial Intelligence, Nanjing University, China

³ Department of Computer Science and Technology, Nanjing University, China

⁴ School of Electronic Science and Engineering, Nanjing University, China

{york_z-xu, sryang}@smail.nju.edu.cn, {blxu, frshen, jianzhao}@nju.edu.cn

Abstract

Existing replay and distillation-based class-incremental learning (CIL) methods are effective at retaining past knowledge but are still constrained by the stability-plasticity dilemma. Since their resulting models are learned over a sequence of incremental tasks, they encode rich representations and can be regarded as pre-trained bases. Building on this view, we propose a plug-in extension paradigm termed Deployment of LoRA Components (DLC) to enhance them. For each task, we use Low-Rank Adaptation (LoRA) to inject task-specific residuals into the base model’s deep layers. During inference, representations with task-specific residuals are aggregated to produce classification predictions. To mitigate interference from non-target LoRA plugins, we introduce a lightweight weighting unit. This unit learns to assign importance scores to different LoRA-tuned representations. Like downloadable content in software, DLC serves as a plug-and-play enhancement that efficiently extends the base methods. Remarkably, on the large-scale ImageNet-100, with merely 4% of the parameters of a standard ResNet-18, our DLC model achieves a significant 8% improvement in accuracy, demonstrating exceptional efficiency. Under a fixed memory budget, methods equipped with DLC surpass state-of-the-art expansion-based methods.

1. Introduction

In recent years, deep learning has achieved remarkable success across a variety of domains [4, 5, 14, 34, 36]. However, most models rely on a key assumption that the data distribution and learned classes remain fixed. In real-world scenarios, data distributions evolve continuously and new classes emerge over time [11], making static training paradigms impractical. Moreover, learning each new task typically re-

lies on additional task-specific sub-models, leading to inefficient model growth over time. Class-Incremental Learning (CIL) [17, 35, 43] thus plays a crucial role in enabling models to continually learn from non-stationary data streams while retaining prior knowledge.

Existing CIL methods [43] can be broadly categorized into rehearsal-based, restriction-based, and expansion-based approaches. Rehearsal-based methods maintain a small replay buffer by storing a limited number of representative exemplars from previous tasks [7, 18, 24]. Other categories of methods likewise adopt rehearsal mechanisms to retain exemplars from past tasks, thereby further improving model accuracy. Expansion-based CIL methods [19, 25, 32] allocate task-specific architectural blocks, creating isolated parameter spaces for new knowledge while freezing previously learned parameters. This strategy alleviates catastrophic forgetting and preserves plasticity on new tasks. However, rather than updating a single model incrementally, these methods expand the network and store, per task, an additional full [33] or partial (about 70%) [40] feature extractor, incurring substantial storage costs. For instance, with ResNet-18, each new task adds about 11.7MB of parameters, roughly equivalent to storing 3,998 images, which is about twice the replay buffer capacity under standard CIL settings. This overhead can limit their practicality for long task sequences, resource-constrained devices, and large-scale deployments.

Restriction-based methods [2, 21] aim to mitigate catastrophic forgetting by constraining model updates on the new task. A representative example is knowledge distillation [23, 26], which preserves previous knowledge by aligning the current model’s output with its earlier versions. These methods perform CIL on a single model, leading to substantially lower storage overhead. As a result, these approaches are practically attractive in real-world settings. However, they inevitably introduce a trade-off [8]:

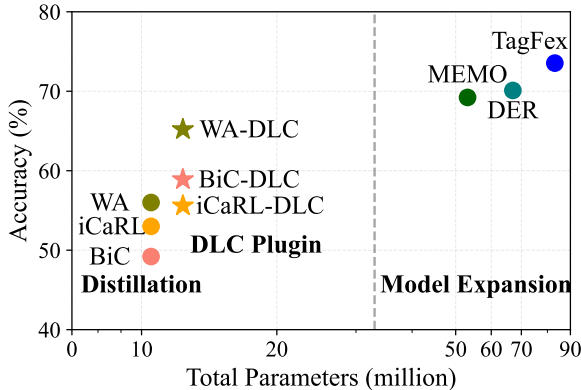


Figure 1. Parameter-accuracy comparison of different CIL methods on ImageNet-100 with ResNet-18. DLC achieves the best balance between parameter efficiency and accuracy compared to prior SOTA methods. iCaRL-DLC, WA-DLC, and BiC-DLC mean integrating DLC into the corresponding methods, respectively.

the model must balance adherence to past knowledge with adaptation to new data. This stability–plasticity dilemma often becomes the key bottleneck for distillation-based approaches. Many enhancements [10, 31, 38] have been proposed to improve their accuracy, yet the core issue persists: distillation and new-task fitting are coupled objectives whose gradients can conflict, leaving performance governed by the same trade-off. A natural way to reduce this interference is to expand extra parameters for new tasks. However, scaling up the feature extractor is quickly parameter-prohibitive, and typical expansion-based schemes retrain task-specific extractors, breaking the shared single-model predictor that distillation relies on. This exposes a new quandary to CIL: *How can we break the stability–plasticity dilemma by introducing a small set of task-specific auxiliary parameters, while remaining friendly to distillation-based methods?*

To address this challenge, we propose the Deployment of LoRA Components (DLC), a plug-and-play extension paradigm for CIL. We revisit parameter-efficient tuning modules in transfer learning beyond the frozen feature extractor assumption, and study them under the training dynamics of replay and distillation-based CIL. We attach task-specific lightweight plugins to deep layers of the base model and instantiate each plugin with LoRA in this work. These plugins provide additional knowledge by injecting residuals into the extracted features. For each incoming task, we first follow the underlying baseline to train the backbone while keeping all plugins frozen, and then update only the plugin associated with the current task. This decoupled update strategy trains each plugin independently, enabling DLC to be deployed into the baseline without interference. During inference, the model activates all plugins to extract their feature representations, which are aggregated for final clas-

sification. However, plugins that are not aligned with the input sample may contribute noisy or weakly informative residuals. We introduce a lightweight weighting unit before the classifier, which automatically assigns importance weights to different plugin outputs. Experimental results on multiple benchmarks show that DLC consistently improves replay and distillation-based baselines. For example, DLC achieves up to 8% accuracy gains on ImageNet-100 with ResNet-18 and on CIFAR-100 with ResNet-32, while increasing the total parameter count by only 4% to 30%. Under the same memory budget, DLC also outperforms existing state-of-the-art CIL baselines. Our contributions are summarized as follows:

- We propose DLC, a plug-and-play plugin extension framework that enables lightweight task-specific plugin residual injection in continually updated backbones, anchored by the consistent knowledge preserved through replay and distillation.
- We introduce a lightweight weighting unit that adaptively suppresses irrelevant plugin activations based on learned importance, reducing feature interference across tasks and leading to more stable and accurate incremental classification.
- Extensive experiments show that DLC significantly boosts various CIL methods’ performance. Meanwhile, under the fixed memory budget, the DLC-enhanced distillation method could surpass SOTA CIL methods.

2. Related Work

2.1. Class Incremental Learning

Class-incremental learning primarily aims to prevent the model from forgetting old classes. Existing methods tackle this challenge from multiple perspectives, including rehearsal [1, 16] that replays representative exemplars from previous classes, regularization [3] or distillation [12] that limit overly aggressive updates on new data, expansion-based designs that train and retain task-specific full [33] or partial [40] feature extractors, and further integrate contrastive objectives [39] to stabilize representations. In addition, some methods leverage transfer learning with Transformers pretrained on large-scale datasets to provide stronger representations [27, 42]. These methods often exhibit an accuracy–memory trade-off: approaches with higher recognition accuracy typically require storing more replay samples or allocating and maintaining additional model parameters through expansion or larger backbones.

2.2. Distillation-Based CIL

Distillation-based CIL trains the model on new tasks while regularizing it to match the predictions of the previous version. A wide range of distillation-based approaches have been explored, including combining distillation with

replay [23], incorporating bias correction [31] or weight alignment [38], momentum-based distillation [20], and plug-and-play auxiliary objectives [10]. Distillation remains appealing as it introduces minimal overhead, can leverage unlabeled incoming samples, and fits a simple single-model training loop, making it broadly applicable in practical settings such as online [30], imbalanced [22], and few-shot [37] CIL. However, the feature extractor’s fixed capacity imposes a fundamental constraint: the model must balance stability and plasticity by trading off classification and distillation losses, ultimately capping achievable accuracy.

3. Preliminaries

3.1. Problem Formulation of CIL

A CIL model aims to learn new classes while retaining previous knowledge from the continuously evolving data streams D_1, D_2, \dots, D_t [8], where $D_i = \{(\mathbf{x}_j, y_j)\}_{j=1}^{n_i}$ containing n_i instances. One class will appear only once on a given D_i and will not be repeated. At each incremental learning stage t , only the current data stream D_t and a few exemplars from the previous classes [23] can be used for model training. For any stage t , the model has learned $D = D_1 \cup D_2 \cup \dots \cup D_t$ streams. We aim to find a model $f(\mathbf{x}) : \mathcal{X} \rightarrow \mathcal{Y}$ that minimizes empirical risk across all learned classes, where \mathcal{X} and $\mathcal{Y} = Y_1 \cup Y_2 \cup \dots \cup Y_t$ represent the sample’s feature and class spaces, respectively. The effectiveness of the model is evaluated by the test dataset $D^{test} = D_1^{test} \cup D_2^{test} \cup \dots \cup D_t^{test}$, which can be expressed in Eq.(1):

$$f^*(\mathbf{x}) = \arg \min_{f \in \mathbb{H}} \mathbb{E}_{(\mathbf{x}, y) \in D^{test}} [\mathbb{I}(f(\mathbf{x}) \neq y)], \quad (1)$$

where \mathbb{H} is the hypothesis space of model and $\mathbb{I}(\cdot)$ denotes the indicator function.

3.2. Consistent Knowledge Preserved in CIL

Considering the classic CIL scenario with only a single feature extractor. The objective function used in non-CIL settings is the cross-entropy loss \mathcal{L}_{CE} , while restriction-based CIL methods incorporate an additional restriction term \mathcal{L}_{MEM} that enforces the preservation of knowledge acquired from previous tasks. This composite objective function can be formally expressed as:

$$\mathcal{L} = \mathcal{L}_{CE} + \mathcal{L}_{MEM}. \quad (2)$$

As a canonical example of restriction-based methods, we examine logit-based distillation, which ensures consistency between the logit distributions produced by the old and new models for known classes. Specifically, the restriction term \mathcal{L}_{MEM} is defined as a distillation loss \mathcal{L}_{KD} . Let $\hat{q}(\mathbf{x})$ and

$q(\mathbf{x})$ represent the logits of the teacher and student models. The cross-entropy version of \mathcal{L}_{KD} is defined as:

$$\mathcal{L}_{KD} = - \sum_i \hat{q}_i(\mathbf{x}) \log(q_i(\mathbf{x})), \quad (3)$$

and the KL divergence version is defined as:

$$\mathcal{L}_{KD} = \tau^2 \sum_i \hat{q}_i(\mathbf{x}) \log\left(\frac{\hat{q}_i(\mathbf{x})}{q_i(\mathbf{x})}\right), \quad (4)$$

where the τ is the temperature scalar.

Moreover, most methods are complemented by a replay buffer that stores a subset of representative exemplars from previous tasks. These exemplars are interleaved with data from the current task during training to help maintain performance on past tasks. Specifically, when learning the t -th task, the model is conventionally trained only on the new dataset D_t . With the replay buffer, the training dataset is supplemented with D_{exp} retrieved from the buffer, forming a combined training set $D_{train} = D_t \cup D_{exp}$.

Although the model’s parameters are dynamically updated throughout the incremental learning process, the use of knowledge distillation and the replay buffer ensures that a portion of knowledge from previous tasks remains preserved. Replay ensures the model continues to minimize the empirical risk on a representative subset of past tasks, anchoring the parameters in regions consistent with previous data. Concurrently, knowledge distillation functions as a functional regularizer, ensuring that the mappings for old classes remain stable by aligning the output logits (or distributions) with those of the prior model. Consequently, a model trained with replay and distillation preserves substantial knowledge of past classes, resulting in a single unified model that is broadly effective but suboptimal. We posit that the knowledge stored in the model can be efficiently activated with minor task-specific parameters.

4. The Proposed Method

DLC proposes a plugin-level residual injection paradigm, as illustrated in Fig. 2. We treat a replay and distillation-trained network as a base model that accumulates knowledge across tasks but remains suboptimal in accuracy, and then augment it with task-specific plugins that inject residual knowledge into the extracted features to improve performance. In this work, each plugin is instantiated with a LoRA-style low-rank parameterization, but is used as a lightweight task extension rather than a conventional fine-tuning update. The proposed DLC is detailed in the following subsections.

4.1. Task-Specific Plugins Deployment

Parameter-efficient tuning is typically used in transfer learning by adapting a feature extractor with frozen parameters,

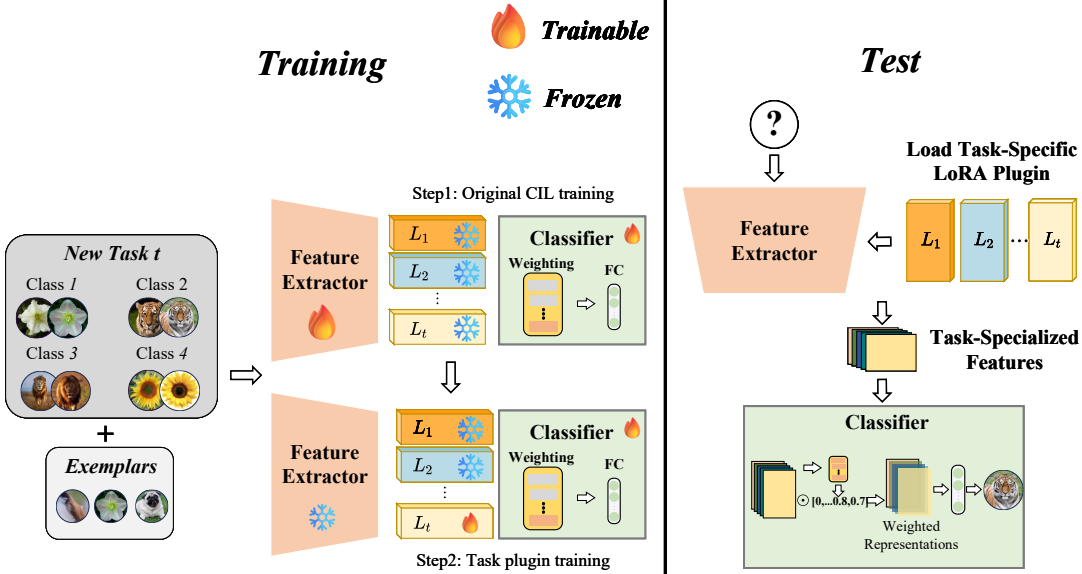


Figure 2. The proposed DLC framework. **Left:** Training. When a new task t arrives, a dedicated plugin set L_t is created. Then sequentially train the feature extractor and L_t . **Right:** Test. The feature extractor sequentially loads all task plugins L_t to produce enhanced representations, which are concatenated, weighted by a gating unit, and classified.

where layer inputs remain largely stationary. Here, we revisit it beyond this static-backbone assumption and study it under replay- and distillation-based class-incremental learning, where old-task outputs are constrained, and intermediate feature drift is therefore controlled during continual updates. Concretely, after training on task t , the output deviation at layer ℓ is bounded by $K_\ell \Gamma_t$ (see Appendix), where K_ℓ depends on hyperparameters such as network structure and distillation temperature, and Γ_t reflects the distribution discrepancy induced by the chosen replay and distillation strategy. This bound directly limits the worst-case feature drift on the old-task distribution, enabling stable optimization of lightweight auxiliary parameters in this dynamic regime.

We introduce a plugin extension design and maintain an independent plugin set for each task. Specifically, for each task t , we create a dedicated set of k plugins for $\phi(\mathbf{x})$, denoted as L_t . The $\phi(\mathbf{x})$ equipped with L_t is denoted by $\phi^{L_t}(\mathbf{x})$. In DLC, plugins are deployed in the final layers of $\phi(\mathbf{x})$. Taking a CNN-based architecture as an example, the first plugin in L_t is attached to the last convolutional layer of $\phi(\mathbf{x})$, and the remaining plugins are placed on progressively earlier layers moving backward through the network. This design is motivated by two considerations. First, deeper features are more semantically meaningful and are directly used for classification, so injecting task-specific residuals at this level can more effectively enhance inter-class discriminability. Second, it is more compatible with distillation-based objectives. If plugins are deployed in shallow layers, residual changes in low-level features would propagate

through the network and amplify logit deviations, increasing the optimization difficulty of distillation losses that rely on output alignment between old and new models.

In DLC, the plugins and $\phi(\mathbf{x})$ undergo a decoupled two-phase training procedure. Specifically, when a new task t arrives, we first train the base model following the underlying baseline procedure, updating only $\phi(\mathbf{x})$ and the classifier \mathbf{W} while keeping all plugins frozen. After this phase, $\phi(\mathbf{x})$ is frozen to prevent knowledge drift, and L_t is trained with the same data. Upon completion, L_t is permanently frozen to safeguard the acquired task-specific knowledge. The training objective for all plugins incorporates the cross-entropy loss and an auxiliary loss [33] commonly used in expansion-style methods, formulated as:

$$\mathcal{L}_{\text{plg}} = \mathcal{L}_{\text{CE}} + \mathcal{L}_{\text{aux}}. \quad (5)$$

The two-phase procedure ensures that plugins are trained without interference from distillation losses, enabling specialized learning for the target task. Since $\phi(\mathbf{x})$ remains frozen during plugin updates, plugin training is stable, and it also prevents the baseline training of $\phi(\mathbf{x})$ from being affected by plugin training, preserving the plug-and-play property of DLC.

During inference, all plugins are activated to extract their respective feature representations. These representations are then concatenated to form an integrated feature vector, which enhances the base model through a multi-task feature ensemble. For a linear classifier \mathbf{W} , the classification process can be formulated as:

$$\hat{y} = \mathbf{W}[\phi^{L_1}(\mathbf{x}), \phi^{L_2}(\mathbf{x}), \dots, \phi^{L_T}(\mathbf{x})] \quad (6)$$

where T denotes the maximum index of known tasks. Notably, we do not need to run the full extractor T times: each plugin injects a residual only at its deployment layer, so the backbone activations up to the earliest deployed layer are shared and computed once, avoiding redundant computation and improving inference efficiency.

4.2. LoRA-Style Residual Plugin

To instantiate each task-specific plugin with minimal parameters, we adopt a LoRA [13]-style low-rank residual parameterization. This design is well-suited for plugin deployment: the rank r provides a simple capacity knob under a fixed budget, the same low-rank residual form applies to both linear and convolutional operators, and the residual structure supports our decoupled training and inference aggregation since plugins can be independently trained, frozen, and combined without modifying the backbone. We emphasize that the backbone weights are kept intact throughout, and the low-rank component is introduced as an auxiliary module that adds a task-specific residual to the feature. That is, the LoRA plugin does not replace or factorize the original weights, but injects additional task knowledge via an additive low-rank branch, which aligns with our plug-and-play deployment setting.

Since most CIL pipelines train CNN-based backbones from scratch, we instantiate the plugin for convolutional operators using a LoRA-style low-rank residual branch (implemented as two convolutions). For a convolutional layer with weight tensor $W_{\text{conv}} \in \mathbb{R}^{C_{\text{out}} \times C_{\text{in}} \times K \times K}$ and input $\mathbf{x} \in \mathbb{R}^{N \times C_{\text{in}} \times H \times W}$, the original forward pass is $\mathbf{h} = W_{\text{conv}} * \mathbf{x}$, where $*$ denotes the convolution operation. The LoRA plugin first processes the input with \mathbf{A} :

$$\mathbf{z} = \mathbf{A} * \mathbf{x}, \quad (7)$$

where $\mathbf{A} \in \mathbb{R}^{r \times C_{\text{in}} \times K \times K}$ projects the feature to a low-rank space. This is followed by \mathbf{B} :

$$\mathbf{h}_{\text{lora}} = \mathbf{B} * \mathbf{z}, \quad (8)$$

where $\mathbf{B} \in \mathbb{R}^{C_{\text{out}} \times r \times 1 \times 1}$ restores the channel dimensionality, and \mathbf{h}_{lora} is added as a residual to the layer output.

In summary, the forward pass of a convolutional layer equipped with the LoRA-style residual plugin is:

$$\mathbf{h}' = W_{\text{conv}} * \mathbf{x} + \frac{\alpha}{r} (\mathbf{B} * (\mathbf{A} * \mathbf{x})), \quad (9)$$

where α is a scaling hyperparameter, and r is the rank.

Compared to the model expansion, instantiating task-specific plugins with a LoRA-style parameterization can bring significant parameter advantages. Specifically, for a convolutional layer (C_{in} , C_{out} , $K \times K$), the space complexity of its parameters is $\Theta(C_{\text{in}}C_{\text{out}}K^2)$, while the plugin only occupies $\Theta(r(C_{\text{in}}K^2 + C_{\text{out}}))$. For expanding

one layer of CNN over T tasks, considering that in a CNN in CIL, C_{out} is generally greater than or equal to C_{in} , we set $C_{\text{in}} = C_{\text{out}} = C$, and K can be regarded as a constant (usually 3 or 7). Since r is low-rank, it can also be regarded as a constant (generally set to 8 or 16). Then, using LoRA-style plugin instantiation reduces the parameter-space complexity of expanding a single CNN layer from $\Theta(TC^2)$ to $\Theta(TC)$. Considering that C is generally between 64 and 512, reducing its order of magnitude from quadratic to linear can substantially reduce the number of parameters.

4.3. Dynamic Weighting Unit

For a sample from task t , all the plugins trained on other tasks are considered non-target plugins. Given that the replay buffer contains only a minimal fraction of the original data for each task, these non-target plugins are not trained on the full data from task t . In particular, plugins trained on tasks 1 to $t-1$ never encounter samples from the task t . Consequently, the residuals extracted by these plugins could be largely irrelevant to the task t , thus introducing uninformative features or even detrimental noise to the classifier.

To mitigate the influence of uninformative residuals from non-target plugins, we will create a weighting unit corresponding to concentrated representations when training on a new task. This unit comprises two linear layers followed by a sigmoid function $\sigma(\cdot)$, denoted as $\omega(\mathbf{x}) = \sigma(\mathbf{W}_2 \text{ReLU}(\mathbf{W}_1 \mathbf{x}))$, $\mathbf{x} \in \mathbb{R}^k$, $\mathbf{W}_1 \in \mathbb{R}^{k \times d}$, $\mathbf{W}_2 \in \mathbb{R}^{d \times k}$, where the sigmoid function normalizes the output to the $[0, 1]$ range, indicating their importance weights. The concatenated representations are passed through this unit before being fed into the classifier, then weighted representations is derived from $\tilde{\mathbf{h}}^{(i)} = \omega^{(i)} \odot \mathbf{h}^{(i)}$, where \odot is element-wise multiplication operator. The weighting unit can be regarded as a gate for the classifier. Jointly trained with the classifier, it helps the model adapt to the high-dimensional feature space and automatically assigns lower weights to uninformative or noisy features.

The automatically trained weighting unit fails to explicitly model the varying importance of representations from different tasks. For a sample i in task t , we denote the representations adapted by LoRA plugins trained on tasks 1 to $t-1$ as $\mathbf{h}_{\text{pre}}^{(i)}$ and those adapted by the remaining LoRA plugins as $\mathbf{h}_{\text{pos}}^{(i)}$, respectively. Then $\mathbf{h}_{\text{pre}}^{(i)}$ should be assigned lower weights as corresponding LoRA plugins were not optimized on task t . However, since the ground-truth task index of each sample is unavailable during the CIL testing, we cannot explicitly control the weighting unit based on task identity. Instead, we employ a supervised regression training to guide the weighting unit to approximate the desired weighting scheme. We decompose the weight $\omega^{(i)}$ for sample i into $[\omega_{\text{pre}}^{(i)}, \omega_{\text{pos}}^{(i)}]$. Then the decision process of the linear

classifier can be rewritten as follows:

$$\mathbf{q}^i = \mathbf{W}_{\text{pre}}(\omega_{\text{pre}}^{(i)} \odot \mathbf{h}_{\text{pre}}^{(i)}) + \mathbf{W}_{\text{pos}}(\omega_{\text{pos}}^{(i)} \odot \mathbf{h}_{\text{pos}}^{(i)}). \quad (10)$$

Formally, the contribution of $\mathbf{h}_{\text{pre}}^{(i)}$ to the classifier's logits can be expressed as $\xi = \mathbf{W}_{\text{pre}}(\omega_{\text{pre}}^{(i)} \odot \mathbf{h}_{\text{pre}}^{(i)})$. To generate effective weights, an importance-aware optimization objective could be incorporated into the training process, denoted as \mathcal{L}_{IA} . This loss function employs the Mean Squared Error (MSE), expressed as follows:

$$\mathcal{L}_{\text{IA}} = \frac{1}{k} \|\omega - \omega_{\text{ideal}}\|_2, \quad (11)$$

where the ω_{ideal} is the ideal weight output, it has $\omega_{\text{ideal-pos}}^{(i)} = 1$ and $\omega_{\text{ideal-pre}}^{(i)} = 0$. In the ideal training case, the model has $\omega_{\text{pos}}^{(i)} \rightarrow 1$ and $\omega_{\text{pre}}^{(i)} \rightarrow 0$, then it has $\mathbb{E}[\xi] \rightarrow 0$ and $\text{Var}[\xi] \rightarrow 0$, so the $\mathbf{h}_{\text{pre}}^{(i)}$ have negligible influence on prediction logits. Even if the ideal scenario is hard to achieve, the classifier can still produce more accurate predictions as long as the representations adapted by reliable plugins are assigned higher weights, while those adapted by non-target plugins are appropriately suppressed. After enabling the weighting unit, \mathcal{L}_{IA} is incorporated into the plugin training, and \mathcal{L}_{plg} in Eq. (5) is extended as follows:

$$\mathcal{L}_{\text{plg}} = \mathcal{L}_{\text{CE}} + \mathcal{L}_{\text{aux}} + \mathcal{L}_{\text{IA}}. \quad (12)$$

5. Experiments

This section conducts extensive experiments. Sec. 5.2 evaluates the validity of DLC on distillation-based baselines. Sec. 5.3 investigates the performance of SOTA CIL methods under the memory-aligned case. Sec. 5.4 evaluates the compatibility of DLC with other data augmentation and plug-and-play loss functions for CIL. Sec. 5.5 analyzes the additional inference overhead introduced by DLC in terms of FLOPs and latency.

5.1. Experimental Setup

Datasets and Split. We chose three benchmark datasets commonly used in CIL, including CIFAR-100 [15], ImageNet-100 [9], and Tiny-ImageNet-200 [28], where the number following the dataset is the total number of classes included. Following the ‘B/Base-m, Inc-n’ rule proposed by [8], we slice each of the above three datasets into CIFAR-100 B10 Inc10, CIFAR-100 B50 Inc10, CIFAR-100 B5 Inc5, ImageNet-100 B50 Inc10, and Tiny-ImageNet B40 Inc40 for the experiment, where m is the number of classes in the first incremental task, and n represents that of every remaining stage. For a fair comparison, we ensure that the training and test datasets are identical for all methods. Detailed information about the dataset is placed in the Appendix section.

Implementation Details. All methods are implemented in PyTorch, with the baseline methods referencing the PyCIL [41], and Gao et al. [10]. We employ the lightweight ResNet-32 tailored for CIFAR datasets on CIFAR-100, while utilizing ResNet-18 for all other benchmark datasets. The optimizer employs SGD with a fixed learning rate of 0.1, incorporating a multi-step schedule. The detailed training hyperparameters, like the optimizer and batch size, largely follow the default settings in PyCIL. All the methods are run using the same random number seed. To eliminate potential confounding effects from increased training epochs, all baselines are run under both the PyCIL-recommended epoch setting and the total epoch budget of DLC’s two-stage training, and the maximum accuracy is reported.

Evaluation Metrics. Following the benchmark protocol settings [23], we use A_b to denote the b -stage accuracy on the test set that includes all known classes after trained with D_1, D_2, \dots, D_b , $\bar{A} = \frac{1}{T} \sum_{b=1}^T A_b$ is average accuracy over T tasks, and A_T is the last accuracy on the test set that includes all learned tasks. We use \bar{A} and A_T to evaluate the model’s performance, which reflects the model’s dynamic learning capacity and generalization ability, respectively.

5.2. Effectiveness on Distillation-Based CIL

In this section, we evaluate the performance improvement brought by the proposed DLC framework across different distillation-based CIL objectives, including iCaRL [23], WA [38], BiC [31], DAKD [12], and MKD [20]. Additionally, a simple herding-based Replay method [23] is included to examine DLC’s contribution in scenarios relying solely on the rehearsal without distillation. We report the \bar{A} and A_T of these established methods with and without DLC across three datasets under varying task configurations. In all experiments, the replay buffer size is fixed at 2,000 exemplars. DLC expands only one LoRA plugin per task, applied to the last convolutional layer of the feature extractor. We also report the total parameters required by DLC and the size of the entire feature extractor for comparison. The results are summarized in Table 1.

The results show that DLC significantly improves all classical replay or distillation-based methods with only one LoRA plugin per task. Moreover, the parameter overhead introduced by DLC is negligible. DLC achieves up to 8% accuracy improvement while expanding only 4.8% to 32% parameters equivalent to the feature extractor, highlighting its practical value in CIL. Fig. 3 shows the confusion matrix heatmap of iCaRL and iCaRL-DLC as an example. DLC increases the thermal intensity along the diagonal for most classes, demonstrating that it could enhance the model’s accuracy across most tasks.

In addition, we compare the final accuracy of DLC-enhanced iCaRL, WA, and BiC with and without the

Table 1. Last performance A_T and average performance \bar{A} comparison. ‘-DLC’ indicates the method using the DLC framework. ‘Extra/Feat #P’ denotes the total number of extra parameters required for deploying DLC and the feature extractor, respectively.

Methods	CIFAR-100				Tiny-ImageNet		ImageNet-100	
	B5 Inc5		B10 Inc10		B50 Inc10		B40 Inc40	
	\bar{A}	A_T	\bar{A}	A_T	\bar{A}	A_T	\bar{A}	A_T
Replay	58.28	38.20	56.82	39.31	51.08	40.88	51.46	37.79
Replay-DLC	58.76	38.69	59.24	41.81	53.72	43.61	51.65	38.66
iCaRL	59.40	39.94	59.67	41.29	55.94	44.44	52.32	36.22
iCaRL-DLC	59.54	41.63	60.06	44.31	56.61	46.35	53.28	39.20
BiC	56.45	32.77	61.14	42.58	53.45	36.04	54.12	39.68
BiC-DLC	58.27	41.07	61.87	43.65	54.46	46.23	54.86	43.09
WA	62.72	45.96	65.82	51.80	65.04	56.94	53.68	39.69
WA-DLC	62.84	46.22	66.79	52.70	65.43	57.71	55.31	43.33
MKD	56.86	36.87	55.73	36.83	46.68	36.17	49.34	34.64
MKD-DLC	57.51	37.33	58.10	40.40	52.18	40.99	50.29	35.75
DAKD	60.01	40.15	60.69	42.32	54.33	43.09	51.98	36.73
DAKD-DLC	60.47	41.54	61.01	43.81	56.99	46.00	52.78	37.38
Extra/Feat #P (MB)	0.15	0.46	0.07	0.46	0.04	0.46	0.45	11.17
							0.52	11.17

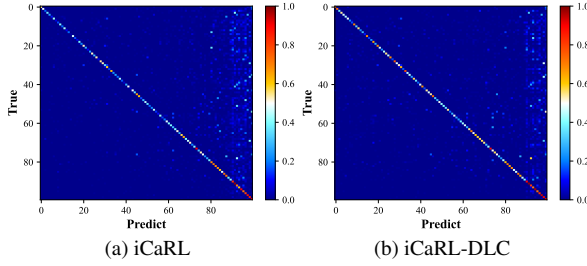


Figure 3. Confusion matrix heatmaps of iCaRL with and w/o DLC on CIFAR-100 B10 Inc10.

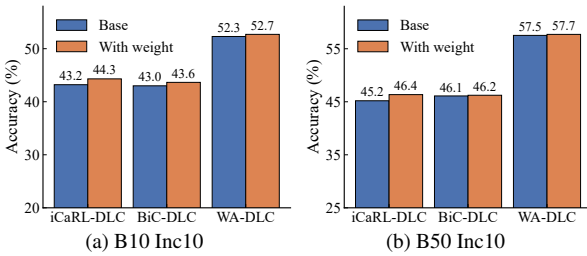


Figure 4. Comparison of A_T with and without the weighting unit for DLC-enhanced methods on CIFAR-100.

weighting unit, as shown in Fig. 4. Results indicate that the proposed weighting unit contributes a certain accuracy gain.

5.3. Comparison under Fixed Memory Budget

Prior research [43] has demonstrated that model-level expansion-based methods achieve state-of-the-art perfor-

Table 2. Performance comparison on CIFAR-100 with aligned memory cost. ‘#P’ represents the number of parameters (million). ‘# ε ’ denotes the number of exemplars, and ‘MS’ denotes the memory size (MB). All methods use ResNet-32 as the backbone.

Method	CIFAR100 B10 Inc10				
	MS	#P	# ε	\bar{A}	A_T
iCaRL	23.5	0.46	7431	70.74	58.12
WA	23.5	0.46	7431	69.25	59.00
BiC	23.5	0.46	7431	70.29	59.20
FOSTER	23.5	0.46	7431	72.18	59.29
DER+WA	23.5	4.60	2000	71.24	60.26
MEMO+WA	23.5	3.62	3312	72.32	61.92
TagFex+WA	23.5	5.62	700	74.00	64.10
WA-DLC	23.5	0.54	7327	75.02	64.79

mance across all standard CIL benchmarks. However, these approaches overlook the substantial memory overhead induced by dynamic architecture growth. Such methods implicitly introduce additional memory budgets, i.e., a model buffer for retaining parameters of the expanded model, which grants them a considerable and unaccounted advantage over other methods that do not store expansion models or adopt more lightweight expansion strategies.

Following the protocol established in [40], this section presents a memory-aligned comparison of CIL baselines. Under a fixed 23.5 MB memory budget, the memory not consumed by a method’s parameters is allocated to replay exemplars. To balance this, methods with fewer parameters store more exemplars, and vice versa. This ensures an equitable evaluation. In addition to the baselines used in Section 5.2, we add several state-of-the-art approaches for

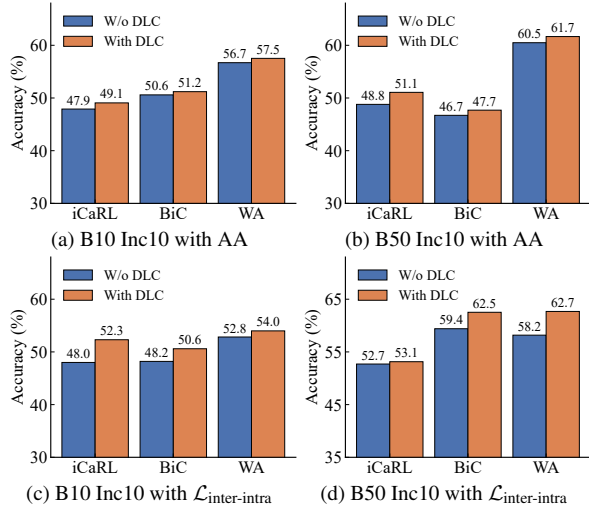


Figure 5. Comparison of A_T with/without DLC on CIFAR-100 when enhanced with AutoAugment (AA) and $\mathcal{L}_{\text{inter-intra}}$.

comprehensive comparison, including FOSTER [29], DER [33], MEMO [40], and TagFex [39]. Among them, DER, MEMO, and TagFex have incorporated the weight alignment from WA in their implementations. As summarized in Table 2, deploying DLC to the distillation-based method WA under the memory-aligned setting yields the highest classification accuracy.

5.4. Compatibility with other Plug-and-Play Enhancements

In addition to DLC, other plug-and-play strategies have been proposed to enhance CIL methods. For example, the data augmentation technique AutoAugment [6] has been employed in the CIFAR-100 dataset by [29, 39]. Meanwhile, two additional training losses $\mathcal{L}_{\text{inter}}$ and $\mathcal{L}_{\text{intra}}$ specifically designed for logit-based distillation methods have been introduced in [10]. This subsection evaluates the compatibility of DLC with such enhanced strategies. Specifically, we compare the accuracy of methods using AutoAugment and the loss $\mathcal{L}_{\text{inter-intra}}$ with and without DLC. For experiments with $\mathcal{L}_{\text{inter-intra}}$, we follow the original implementation and use ResNet-18 as the backbone. As shown in the Fig. 5, DLC consistently brings significant improvements, demonstrating its compatibility with other plug-and-play enhancements.

5.5. Additional Computational Overhead from DLC

This section investigates the additional inference cost introduced by deploying DLC. Using iCaRL as a representative baseline, we evaluate two deployment variants: iCaRL equipped with one LoRA plugin per task, and iCaRL equipped with both the LoRA plugins and the weighting

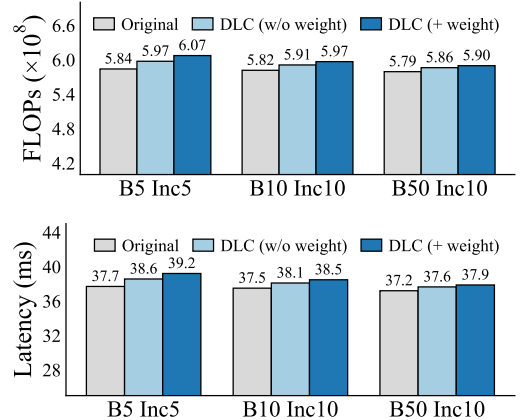


Figure 6. Comparison of inference FLOPs and per-sample inference latency with and w/o DLC under different task settings.

unit. Concretely, on ImageNet-100, we report the total FLOPs and the average inference latency per sample (ms) measured on the same test set. The results are shown in Fig. 6. Overall, neither FLOPs nor latency increases substantially as the number of tasks grows. Instead, both grow mildly as the task sequence extends. Even under long sequences such as B5 Inc5, the increases in FLOPs and inference time are only about 4%. These results indicate that DLC provides a lightweight and computation-friendly parameter extension for enhancing distillation-based CIL.

6. Conclusion

In this work, we address a challenge in distillation-based class-incremental learning: improving the model performance with only a small amount of task-specific auxiliary parameters, without breaking the single-model distillation setting. We propose DLC, a plug-and-play plugin extension framework that augments replay and distillation-based baselines with task-specific LoRA-style residual plugins. DLC trains each plugin in a decoupled manner and then freezes it, which both avoids interference from distillation objectives and preserves the acquired task knowledge. We further introduce a lightweight weighting unit to down-weight irrelevant plugin features at inference. Extensive experiments demonstrate that DLC consistently improves replay and distillation-based CIL baselines with few parameter overhead. Future work will explore more expressive weighting designs for stronger feature integration, as well as earlier-layer plugin deployment to further improve adaptability.

References

- [1] Agil Aghasianli, Yi Li, and Plamen Angelov. Prototype-based continual learning with label-free replay buffer and cluster

- preservation loss. In *Proceedings of the Computer Vision and Pattern Recognition Conference*, pages 6545–6554, 2025. 2
- [2] Hongjoon Ahn, Sungmin Cha, Donggyu Lee, and Taesup Moon. Uncertainty-based continual learning with adaptive regularization. *Advances in neural information processing systems*, 32, 2019. 1
- [3] Ang Bian, Wei Li, Hangjie Yuan, Mang Wang, Zixiang Zhao, Aojun Lu, Pengliang Ji, Tao Feng, et al. Make continual learning stronger via c-flat. *Advances in Neural Information Processing Systems*, 37:7608–7630, 2024. 2
- [4] Shuo Chen, Gang Niu, Chen Gong, Jun Li, Jian Yang, and Masashi Sugiyama. Large-margin contrastive learning with distance polarization regularizer. In *International Conference on Machine Learning*, pages 1673–1683. PMLR, 2021. 1
- [5] Shuo Chen, Chen Gong, Jun Li, Jian Yang, Gang Niu, and Masashi Sugiyama. Learning contrastive embedding in low-dimensional space. *Advances in Neural Information Processing Systems*, 35:6345–6357, 2022. 1
- [6] Ekin D Cubuk, Barret Zoph, Dandelion Mane, Vijay Vasudevan, and Quoc V Le. Autoaugment: Learning augmentation policies from data. *arXiv preprint arXiv:1805.09501*, 2018. 8
- [7] Matthias De Lange and Tinne Tuytelaars. Continual prototype evolution: Learning online from non-stationary data streams. In *Proceedings of the IEEE/CVF international conference on computer vision*, pages 8250–8259, 2021. 1
- [8] Matthias De Lange, Rahaf Aljundi, Marc Masana, Sarah Parisot, Xu Jia, Aleš Leonardis, Gregory Slabaugh, and Tinne Tuytelaars. A continual learning survey: Defying forgetting in classification tasks. *IEEE transactions on pattern analysis and machine intelligence*, 44(7):3366–3385, 2021. 1, 3, 6
- [9] Jia Deng, Wei Dong, Richard Socher, Li-Jia Li, Kai Li, and Li Fei-Fei. Imagenet: A large-scale hierarchical image database. In *2009 IEEE conference on computer vision and pattern recognition*, pages 248–255. Ieee, 2009. 6
- [10] Zijian Gao, Shanhai Han, Xingxing Zhang, Kele Xu, Dulan Zhou, Xinjun Mao, Yong Dou, and Huaimin Wang. Maintaining fairness in logit-based knowledge distillation for class-incremental learning. In *Proceedings of the AAAI Conference on Artificial Intelligence*, pages 16763–16771, 2025. 2, 3, 6, 8
- [11] Heitor Murilo Gomes, Jean Paul Barddal, Fabrício Enembreck, and Albert Bifet. A survey on ensemble learning for data stream classification. *ACM Computing Surveys (CSUR)*, 50(2):1–36, 2017. 1
- [12] Jiangpeng He. Gradient reweighting: Towards imbalanced class-incremental learning. In *Proceedings of the IEEE/CVF Conference on Computer Vision and Pattern Recognition*, pages 16668–16677, 2024. 2, 6
- [13] Edward J Hu, Yelong Shen, Phillip Wallis, Zeyuan Allen-Zhu, Yuanzhi Li, Shean Wang, Lu Wang, Weizhu Chen, et al. Lora: Low-rank adaptation of large language models. *ICLR*, 1(2):3, 2022. 5
- [14] Alejandro Jaimes and Nicu Sebe. Multimodal human-computer interaction: A survey. *Computer vision and image understanding*, 108(1-2):116–134, 2007. 1
- [15] Alex Krizhevsky, Geoffrey Hinton, et al. Learning multiple layers of features from tiny images. *Technical report*, 2009. 6
- [16] Yichen Li, Haozhao Wang, Yining Qi, Wei Liu, and Ruixuan Li. Re-fed+: A better replay strategy for federated incremental learning. *IEEE Transactions on Pattern Analysis and Machine Intelligence*, 2025. 2
- [17] Yan-Shuo Liang and Wu-Jun Li. Loss decoupling for task-agnostic continual learning. *Advances in Neural Information Processing Systems*, 36:11151–11167, 2024. 1
- [18] David Lopez-Paz and Marc'Aurelio Ranzato. Gradient episodic memory for continual learning. *Advances in neural information processing systems*, 30, 2017. 1
- [19] Arun Mallya, Dillon Davis, and Svetlana Lazebnik. Piggyback: Adapting a single network to multiple tasks by learning to mask weights. In *Proceedings of the European conference on computer vision (ECCV)*, pages 67–82, 2018. 1
- [20] Nicolas Michel, Maorong Wang, Ling Xiao, and Toshihiko Yamasaki. Rethinking momentum knowledge distillation in online continual learning. In *International Conference on Machine Learning*, pages 35607–35622. PMLR, 2024. 3, 6
- [21] Cuong V Nguyen, Yingzhen Li, Thang D Bui, and Richard E Turner. Variational continual learning. *arXiv preprint arXiv:1710.10628*, 2017. 1
- [22] Milad Khademi Nori, Il-Min Kim, and Guanghui Wang. Federated class-incremental learning: A hybrid approach using latent exemplars and data-free techniques to address local and global forgetting. *arXiv preprint arXiv:2501.15356*, 2025. 3
- [23] Sylvestre-Alvise Rebuffi, Alexander Kolesnikov, Georg Sperl, and Christoph H Lampert. icarl: Incremental classifier and representation learning. In *Proceedings of the IEEE conference on Computer Vision and Pattern Recognition*, pages 2001–2010, 2017. 1, 3, 6
- [24] David Rolnick, Arun Ahuja, Jonathan Schwarz, Timothy Lillicrap, and Gregory Wayne. Experience replay for continual learning. *Advances in neural information processing systems*, 32, 2019. 1
- [25] Joan Serra, Didac Suris, Marius Miron, and Alexandros Karatzoglou. Overcoming catastrophic forgetting with hard attention to the task. In *International conference on machine learning*, pages 4548–4557. PMLR, 2018. 1
- [26] Christian Simon, Piotr Koniusz, and Mehrtash Harandi. On learning the geodesic path for incremental learning. In *Proceedings of the IEEE/CVF conference on Computer Vision and Pattern Recognition*, pages 1591–1600, 2021. 1
- [27] Hai-Long Sun, Da-Wei Zhou, Hanbin Zhao, Le Gan, De-Chuan Zhan, and Han-Jia Ye. Mos: Model surgery for pre-trained model-based class-incremental learning. In *Proceedings of the AAAI Conference on Artificial Intelligence*, pages 20699–20707, 2025. 2
- [28] Oriol Vinyals, Charles Blundell, Timothy Lillicrap, Daan Wierstra, et al. Matching networks for one shot learning. *Advances in neural information processing systems*, 29, 2016. 6
- [29] Fu-Yun Wang, Da-Wei Zhou, Han-Jia Ye, and De-Chuan Zhan. Foster: Feature boosting and compression for class-

- incremental learning. In *European conference on computer vision*, pages 398–414. Springer, 2022. 8
- [30] Maorong Wang, Nicolas Michel, Ling Xiao, and Toshihiko Yamasaki. Improving plasticity in online continual learning via collaborative learning. In *Proceedings of the IEEE/CVF Conference on Computer Vision and Pattern Recognition*, pages 23460–23469, 2024. 3
- [31] Yue Wu, Yinpeng Chen, Lijuan Wang, Yuancheng Ye, Zicheng Liu, Yandong Guo, and Yun Fu. Large scale incremental learning. In *Proceedings of the IEEE/CVF conference on computer vision and pattern recognition*, pages 374–382, 2019. 2, 3, 6
- [32] Ju Xu and Zhanxing Zhu. Reinforced continual learning. *Advances in neural information processing systems*, 31, 2018. 1
- [33] Shipeng Yan, Jiangwei Xie, and Xuming He. Der: Dynamically expandable representation for class incremental learning. In *Proceedings of the IEEE/CVF conference on computer vision and pattern recognition*, pages 3014–3023, 2021. 1, 2, 4, 8
- [34] Suorong Yang, Furao Shen, and Jian Zhao. Entaument: Entropy-driven adaptive data augmentation framework for image classification. In *European Conference on Computer Vision*, pages 197–214. Springer, 2024. 1
- [35] Suorong Yang, Tianyue Zhang, Zhiming Xu, Peijia Li, Baile Xu, Furao Shen, and Jian Zhao. Supervised contrastive learning with prototype distillation for data incremental learning. *Neural Networks*, page 107651, 2025. 1
- [36] Han-Jia Ye, De-Chuan Zhan, Nan Li, and Yuan Jiang. Learning multiple local metrics: Global consideration helps. *IEEE transactions on pattern analysis and machine intelligence*, 42(7):1698–1712, 2019. 1
- [37] Jiaxing Zeng, Yifeng Tan, Lina Yang, Siwei Zhang, and Lianhui Liang. Terrasap: Spatially aware prompt-based framework for few-shot class-incremental learning in remote sensing image classification. *IEEE Journal of Selected Topics in Applied Earth Observations and Remote Sensing*, 19: 3143–3156, 2025. 3
- [38] Bowen Zhao, Xi Xiao, Guojun Gan, Bin Zhang, and Shu-Tao Xia. Maintaining discrimination and fairness in class incremental learning. In *Proceedings of the IEEE/CVF conference on computer vision and pattern recognition*, pages 13208–13217, 2020. 2, 3, 6
- [39] Bowen Zheng, Da-Wei Zhou, Han-Jia Ye, and De-Chuan Zhan. Task-agnostic guided feature expansion for class-incremental learning. In *Proceedings of the Computer Vision and Pattern Recognition Conference*, pages 10099–10109, 2025. 2, 8
- [40] Da-Wei Zhou, Qi-Wei Wang, Han-Jia Ye, and De-Chuan Zhan. A model or 603 exemplars: Towards memory-efficient class-incremental learning. *arXiv preprint arXiv:2205.13218*, 2022. 1, 2, 7, 8
- [41] Da-Wei Zhou, Fu-Yun Wang, Han-Jia Ye, and De-Chuan Zhan. Pycil: a python toolbox for class-incremental learning, 2023. 6
- [42] Da-Wei Zhou, Hai-Long Sun, Han-Jia Ye, and De-Chuan Zhan. Expandable subspace ensemble for pre-trained model-based class-incremental learning. In *Proceedings of the IEEE/CVF Conference on Computer Vision and Pattern Recognition*, pages 23554–23564, 2024. 2
- [43] Da-Wei Zhou, Qi-Wei Wang, Zhi-Hong Qi, Han-Jia Ye, De-Chuan Zhan, and Ziwei Liu. Class-incremental learning: A survey. *IEEE Transactions on Pattern Analysis and Machine Intelligence*, 2024. 1, 7

Appendix

A. Dataset Description

CIFAR-100 CIFAR-100 (Canadian Institute for Advanced Research 100-class dataset) is a widely used standard benchmark dataset in the field of computer vision, particularly for image classification tasks. It is an expanded version of the CIFAR-10 dataset, curated by the Canadian Institute for Advanced Research. A defining feature of this dataset is its fine-grained categorical structure. It contains a total of 100 distinct fine-grained classes (fine labels), organized hierarchically under 20 broader superclasses (coarse labels), with each superclass encompassing precisely 5 fine-grained classes. This hierarchical organization provides a valuable foundation for researching multi-level classification. The dataset comprises 60,000 tiny color images, each with a fixed resolution of 32x32 pixels. This compact size makes the dataset manageable for rapid experimentation and algorithm iteration, while simultaneously presenting significant challenges for model recognition capabilities due to the extreme low resolution. The 60,000 images are explicitly divided into 50,000 training images and 10,000 test images, meaning each fine-grained class includes 500 training images and 100 test images. CIFAR-100 offers broad and diverse category coverage, encompassing common objects (various vehicles, furniture, appliances), animals (mammals, fish, insects), plants (flowers, trees), and natural scenes (mountains, oceans), among others. Its extensive number of classes combined with its moderate scale make it an ideal testbed for evaluating and comparing the performance and generalization capabilities of image classification models—especially Convolutional Neural Networks (CNNs)—as well as for exploring advanced tasks like few-shot learning and transfer learning.

ImageNet-100 ImageNet-100 is a commonly used subset of the well-known large-scale image dataset, ImageNet. Its purpose is to significantly reduce computational resource requirements and training time while preserving much of ImageNet's richness and challenge, making it more suitable for rapid prototyping, algorithm exploration, and research in resource-constrained environments. As the name implies, ImageNet-100 consists of 100 classes (synsets) selected from the original ImageNet dataset. The selection of these classes is typically not entirely random; it often follows specific strategies (e.g., choosing semantically distinct classes or classes with relatively higher sample counts) to ensure the subset remains representative and diverse. The dataset contains approximately 100,000 high-resolution color images curated from these 100 classes. This represents a substantial reduction in scale compared to the millions of images in the full ImageNet. The standard partition of the dataset usually includes a training set and a validation set. The training set contains roughly 1,000 images per class, totaling approximately 100,000 images. The validation set contains about 50 images per class, totaling around 5,000 images. The images themselves are typically of variable sizes (significantly larger than CIFAR's 32x32 pixels) and require preprocessing (like cropping and resizing) before being fed into models. ImageNet-100 inherits core characteristics from its parent dataset: rich and realistic image content, high semantic distinction between classes, significant intra-class variation (the same object under different viewpoints, lighting, occlusion), and inter-class similarities. It is widely used for training and evaluating image classification models, as well as for transfer learning tasks. Compared to smaller datasets like CIFAR, models pre-trained on ImageNet-100 generally learn more generalizable visual features suitable for fine-tuning on downstream tasks. Compared to the full ImageNet, it offers faster iteration cycles and lower hardware barriers to entry.

TinyImageNet-200 TinyImageNet-200 is a downsized variant of the ImageNet dataset, specifically created for educational and experimental purposes in deep learning and computer vision research. It features a curated subset of 200 distinct object categories (synsets) carefully selected from the full ImageNet hierarchy. The dataset contains roughly 100,000 high-resolution color images – significantly fewer than its parent dataset but substantially more than smaller benchmarks like CIFAR. Each image in Tiny ImageNet has been consistently downsampled and cropped to a fixed resolution of 64x64 pixels, maintaining a usable size while greatly reducing computational demands compared to processing full-sized ImageNet images. The dataset comes with a predefined partition: a training set containing 500 images per class, a separate validation set with 50 images per class, and a test set also containing 50 images per class, totaling approximately 100,000 training images, 10,000 validation images, and 10,000 test images. Alongside the images, TinyImageNet provides essential metadata files including a `wnids.txt` file listing the WordNet IDs for all 200 classes, a `words.txt` file mapping these IDs to human-readable labels, and a structured `val_annotations.txt` file listing the ground-truth classes for validation images. Its manageable scale, balanced class representation, and standardized structure make Tiny ImageNet-200 a popular choice for academic courses exploring deep learning architectures (particularly CNNs and Vision Transformers), as well as for research prototyping on tasks such as image classification, transfer learning, and model robustness evaluation, especially where computational resources are constrained but larger challenges than CIFAR are needed.

B. Feature Drift Bounds under Logit Distillation and Herding Replay

Before applying methods like LoRA to continually updated models, it is imperative to guarantee that the feature extractor's output deviation for previous tasks remains bounded before and after training. Otherwise, if catastrophic forgetting causes a significant shift in outputs, the plugin modules would be unable to extract meaningful residuals.

Setting. Consider a sequence of tasks D_1, D_2, \dots, D_t . At task t , the model is trained on

$$D_{\text{train}} = D_t \cup D_{\text{exp}}, \quad (13)$$

where D_{exp} is the class-balanced exemplar set from previous tasks based on the herding replay strategy in iCaRL. Let θ denote the parameters of a convolutional feature extractor $\phi(\mathbf{x})$, and let $h_\ell(x; \theta) \in \mathbb{R}^{d_\ell}$ denote the output of layer ℓ in $\phi(\mathbf{x})$. We denote the parameters of $\phi(\mathbf{x})$ as θ_{t-1} and θ_t for before and after training on task t .

We adopt the logit-based distillation approach as a representative case for analysis. To constrain forgetting, the logits are distilled from the teacher to the student. The logits of teacher and student are denoted as $\hat{z}(x)$ and $z(x)$. For temperature $T > 0$, define the softened probabilities

$$\hat{q}^T(x) = \text{softmax}(\hat{z}(x)/T), \quad (14)$$

$$q^T(x) = \text{softmax}(z(x)/T). \quad (15)$$

The cross-entropy-based distillation loss is

$$\mathcal{L}_{\text{KD}}(x) = - \sum_{i=1}^C \hat{q}_i^T(x) \log q_i^T(x) \quad (16)$$

$$= H(\hat{q}^T(x)) + \text{KL}(\hat{q}^T(x) \| q^T(x)). \quad (17)$$

Where $H(\hat{q}^T(x))$ denotes the Shannon entropy of the teacher distribution,

$$H(\hat{q}^T(x)) := - \sum_{i=1}^C \hat{q}_i^T(x) \log \hat{q}_i^T(x),$$

so the KD loss decomposes into the teacher's entropy and the KL divergence between the teacher and the student.

The empirical distillation loss over D_{exp} is

$$\bar{\mathcal{L}}_{\text{KD}} = \frac{1}{|D_{\text{exp}}|} \sum_{x \in D_{\text{exp}}} \mathcal{L}_{\text{KD}}(x). \quad (18)$$

It serves as a measurable proxy for how closely the student imitates the teacher on the subset of old-task samples preserved through herding replay.

Our goal is to study how much the intermediate-layer features drift after learning on a new task. For any layer ℓ , define the drift as:

$$\Delta h_\ell(x) = h_\ell(x; \theta_t) - h_\ell(x; \theta_{t-1}). \quad (19)$$

which quantifies the amount by which the feature extractor changes its representation of an old-task sample. Bounding this is crucial for ensuring that LoRA plugins trained on earlier feature distributions remain effective after the model is updated on new tasks.

In addition, to compare logits in a way that reflects changes in their meaningful structure rather than arbitrary additive shifts, we use centered logits:

$$\bar{z}(x) = z(x) - \frac{1}{C} \sum_{k=1}^C z_k(x) \mathbf{1}, \quad (20)$$

$$\bar{\hat{z}}(x) = \hat{z}(x) - \frac{1}{C} \sum_{k=1}^C \hat{z}_k(x) \mathbf{1}. \quad (21)$$

Centered logit is necessary because logits are defined only up to a constant offset: adding a constant to all logit entries leaves the softmax distribution unchanged. By removing this offset, we ensure that the norms of logit differences reflect genuine changes in class-relative predictions rather than uninformative bias shifts. This step allows the later Lipschitz bounds to connect logit discrepancies with feature discrepancies in a well-defined way.

Assumptions

A1 (Non-degenerate teacher distribution). There exists $\delta \in (0, 1/C]$ that satisfies:

$$\hat{q}_i^T(x) \geq \delta \quad \text{for all } x \in D_{\text{exp}} \text{ and } i. \quad (22)$$

This condition prevents extreme logit sharpness and ensures the log-softmax function is well-conditioned. The assumption is directly satisfied in standard knowledge distillation settings. In particular, the use of a temperature parameter $T > 1$ produces softened teacher probabilities,

$$\hat{q}_i^T(x) = \frac{\exp(\hat{z}_i(x)/T)}{\sum_j \exp(\hat{z}_j(x)/T)},$$

which guarantees that no class probability collapses to zero. Alternatively, label smoothing also enforces a uniform lower bound on class probabilities. Thus, **A1** follows from standard KD practice and is not a restrictive condition.

A2 (Local bi-Lipschitz continuity). Let Φ_ℓ denote the mapping from the ℓ -th layer feature to the centered logits \bar{z} through subsequent layers. There exist constants $0 < \mu_\ell \leq L_\ell < \infty$ such that

$$\mu_\ell \|u - v\|_2 \leq \|\Phi_\ell(u) - \Phi_\ell(v)\|_2 \leq L_\ell \|u - v\|_2, \quad (23)$$

for all u, v within a neighborhood of past-task features in D_{exp} . This ensures logits and features change proportionally, which is well supported by the structure of modern neural networks. Convolutional layers, affine transformations, and common nonlinearities (ReLU, SiLU, GELU) are all Lipschitz continuous. Since compositions of Lipschitz functions remain Lipschitz, the entire feature-to-logit map possesses an upper Lipschitz constant. The lower Lipschitz constant reflects local non-collapse of the representation: empirically, trained deep networks do not map distinct inputs from the same manifold region to identical logits. Similar assumptions have been used in analyses of embedding stability and invertibility of deep models. Therefore, **A2** expresses a standard geometric regularity of neural networks rather than a special structural requirement.

A3 (Empirical KD value). At the end of training, the empirical KD loss over D_{exp} equals \bar{L}_{KD} . This is not an additional assumption but rather a definition of the observable optimization outcome. The analysis treats \bar{L}_{KD} as a known scalar summarizing how well the student matches the teacher on replay samples.

A4 (Generalization from herded exemplars). The replay buffer D_{exp} maintains an equal number of samples per class, and $\mathcal{L}_{\text{KD}}(x) \in [0, \log C]$ is bounded, so with probability at least $1 - \delta_0$, we have:

$$|\mathbb{E}_{x \sim \mathcal{D}_{<t}} [\mathcal{L}_{\text{KD}}(x)] - \bar{L}_{\text{KD}}| \leq \epsilon_{\text{gen}}, \quad (24)$$

$$\epsilon_{\text{gen}} = O\left(\sqrt{\frac{\log(1/\delta_0)}{|D_{\text{exp}}|}}\right), \quad (25)$$

where $\mathcal{D}_{<t}$ is the joint distribution of all previous tasks. This assumption holds because the following properties guarantee that the empirical distillation loss concentrates around its population expectation. The boundedness of the distillation loss,

$$0 \leq \mathcal{L}_{\text{KD}}(x) \leq \log C,$$

implies that empirical averages of \mathcal{L}_{KD} satisfy standard concentration inequalities. Moreover, the herding procedure constructs D_{exp} as a class-balanced set that approximates class means in feature space, making it an approximately representative subset of the past-task distribution $\mathcal{D}_{<t}$. As a result, the empirical quantity

$$\bar{L}_{\text{KD}} = \frac{1}{|D_{\text{exp}}|} \sum_{x \in D_{\text{exp}}} \mathcal{L}_{\text{KD}}(x)$$

forms a low-variance estimator of the population expectation. Applying Hoeffding-type bounds for bounded losses yields, with probability at least $1 - \delta_0$,

$$|\mathbb{E}_{x \sim \mathcal{D}_{<t}} [\mathcal{L}_{\text{KD}}(x)] - \bar{L}_{\text{KD}}| \leq O\left(\sqrt{\frac{\log(1/\delta_0)}{|D_{\text{exp}}|}}\right),$$

Auxiliary Lemmas

Lemma 1 (KD controls probability discrepancy). For any x , by Pinsker's inequality:

$$\|q^T(x) - \hat{q}^T(x)\|_1 \leq \sqrt{2 \text{KL}(\hat{q}^T(x) \| q^T(x))} \leq \sqrt{2(\mathcal{L}_{\text{KD}}(x) - H(\hat{q}^T(x)))}. \quad (26)$$

Averaging this equation over D_{exp} gives

$$\frac{1}{|D_{\text{exp}}|} \sum_{x \in D_{\text{exp}}} \|q^T(x) - \hat{q}^T(x)\|_1 \leq \sqrt{2 \left(\bar{L}_{\text{KD}} - \frac{1}{|D_{\text{exp}}|} \sum_x H(\hat{q}^T(x)) \right)}.$$

Lemma 2 (Probability discrepancy controls logit discrepancy). Softmax relates logits and probabilities by:

$$(z_i - z_j) = T \log \left(\frac{q_i^T}{q_j^T} \right). \quad (27)$$

So under **A1**, for any $i \neq j$, Because of Lipschitz continuity of $\log p$ over a bounded domain, differences in log-probabilities are linearly bounded by differences in probabilities:

$$|\log q_i^T - \log \hat{q}_i^T| \leq \frac{T}{\delta} (|q_i^T - \hat{q}_i^T|). \quad (28)$$

So it has:

$$|(z_i - z_j) - (\hat{z}_i - \hat{z}_j)| = T \left| \log \frac{q_i^T}{q_j^T} - \log \frac{\hat{q}_i^T}{\hat{q}_j^T} \right| \quad (29)$$

$$\leq \frac{T}{\delta} (|q_i^T - \hat{q}_i^T| + |q_j^T - \hat{q}_j^T|). \quad (30)$$

Therefore,

$$\|\bar{z}(x) - \hat{z}(x)\|_2 \leq \frac{T}{\delta} \|q^T(x) - \hat{q}^T(x)\|_1. \quad (31)$$

Averaging Eq.(31) over D_{exp} and combining it with Eq. (27) in **Lemma 1** yields:

$$\frac{1}{|D_{\text{exp}}|} \sum_{x \in D_{\text{exp}}} \|\bar{z}(x) - \hat{z}(x)\|_2 \leq \frac{T}{\delta} \sqrt{2 \left(\bar{L}_{\text{KD}} - \frac{1}{|D_{\text{exp}}|} \sum_x H(\hat{q}^T(x)) \right)}. \quad (32)$$

Lemma 3. Under **A2**, for any x , it has:

$$\mu_\ell \|h_\ell(x; \theta_t) - h_\ell(x; \theta_{t-1})\|_2 \leq \|\bar{z}(x) - \hat{z}(x)\|_2 \quad (33)$$

$$\leq L_\ell \|h_\ell(x; \theta_t) - h_\ell(x; \theta_{t-1})\|_2. \quad (34)$$

Main Conclusions

Theorem 1 (Empirical bound on feature drift). For any layer ℓ ,

$$\frac{1}{|D_{\text{exp}}|} \sum_{x \in D_{\text{exp}}} \|h_\ell(x; \theta_t) - h_\ell(x; \theta_{t-1})\|_2 \leq \frac{T}{\mu_\ell \delta} \sqrt{2 \left(\bar{L}_{\text{KD}} - \frac{1}{|D_{\text{exp}}|} \sum_x H(\hat{q}^T(x)) \right)}. \quad (35)$$

Proof. This conclusion can be straightforwardly proved by combining the Eq.(33) in **Lemma 3** (first averaging it over D_{exp}) with the Eq.(32) of **Lemma 2**.

Theorem 2 (Distributional bound over past-task distribution). Under **A1–A4**, with probability at least $1 - \delta_0$,

$$\mathbb{E}_{x \sim \mathcal{D}_{< t}} \|h_\ell(x; \theta_t) - h_\ell(x; \theta_{t-1})\|_2 \leq \frac{T}{\mu_\ell \delta} \sqrt{2 \left(\bar{L}_{\text{KD}} - \mathbb{E}_{x \sim \mathcal{D}_{< t}} [H(\hat{q}^T(x))] + \epsilon_{\text{gen}} \right)}. \quad (36)$$

Proof. The expectation form of **Lemma 2** states that

$$\mathbb{E}_{x \sim \mathcal{D}_{<t}} \|\bar{z}(x) - \bar{\bar{z}}(x)\|_2 \leq \frac{T}{\delta} \sqrt{2 \left(\mathbb{E}_{x \sim \mathcal{D}_{<t}} \mathcal{L}_{\text{KD}}(x) - \mathbb{E}_{x \sim \mathcal{D}_{<t}} H(\hat{q}^T(x)) \right)}. \quad (37)$$

A4 ensures that the empirical distillation loss generalizes to the past-task distribution:

$$\left| \mathbb{E}_{x \sim \mathcal{D}_{<t}} \mathcal{L}_{\text{KD}}(x) - \bar{L}_{\text{KD}} \right| \leq \epsilon_{\text{gen}}. \quad (38)$$

Hence,

$$\mathbb{E}_{x \sim \mathcal{D}_{<t}} \mathcal{L}_{\text{KD}}(x) \leq \bar{L}_{\text{KD}} + \epsilon_{\text{gen}}. \quad (39)$$

Substituting this into Eq.(37) yields:

$$\mathbb{E}_{x \sim \mathcal{D}_{<t}} \|\bar{z}(x) - \bar{\bar{z}}(x)\|_2 \leq \frac{T}{\delta} \sqrt{2 \left(\bar{L}_{\text{KD}} - \mathbb{E}_{x \sim \mathcal{D}_{<t}} H(\hat{q}^T(x)) + \epsilon_{\text{gen}} \right)}. \quad (40)$$

Lemma 3 states that for every x ,

$$\mu_\ell \|h_\ell(x; \theta_t) - h_\ell(x; \theta_{t-1})\|_2 \leq \|\bar{z}(x) - \bar{\bar{z}}(x)\|_2. \quad (41)$$

Taking expectation on both sides gives:

$$\mathbb{E}_{x \sim \mathcal{D}_{<t}} \|h_\ell(x; \theta_t) - h_\ell(x; \theta_{t-1})\|_2 \leq \frac{1}{\mu_\ell} \mathbb{E}_{x \sim \mathcal{D}_{<t}} \|\bar{z}(x) - \bar{\bar{z}}(x)\|_2. \quad (42)$$

Then the conclusion to be proved can be obtained by combining Eq.(40) with Eq.(42).

Theorems 1–2 imply

$$\mathbb{E} \|\Delta h_\ell(x)\| \leq \underbrace{\frac{T}{\mu_\ell \delta}}_{\text{constant } K_\ell} \times \underbrace{\sqrt{2(\Delta_{\text{KD}} + \epsilon_{\text{gen}})}}_{\text{variable } \Gamma_t}, \quad (43)$$

where $\Delta_{\text{KD}} = \mathbb{E}[\mathcal{L}_{\text{KD}}(x) - H(\hat{q}^T(x))]$ reflects the effectiveness of distillation on the data of previous tasks. A smaller Δ_{KD} represents the predictive behavior of the student model that aligns with that of the teacher model on these tasks. $\epsilon_{\text{gen}} = O(\sqrt{\log(1/\delta_0)/|D_{\text{exp}}|})$ decreases as more exemplars are stored. The constant $\frac{T}{\mu_\ell \delta}$ depends on network smoothness and temperature parameters. The K_ℓ captures the conditioning of the feature-to-logit map and the softness of the teacher distribution, while the Γ_t measures how much logit drift the distillation and replay objective permits.

This bound shows that when distillation is optimized and the exemplars approximate the old-task distribution well, the deep feature representations of past data remain stable even as the model learns new tasks. Therefore, even though $\phi(\mathbf{x})$ continuously updates its parameters, the output of each layer for previous tasks remains relatively stable. This allows the plugins trained on earlier tasks to stay effective, thereby enabling the deployment of DLC in replay- and distillation-based CIL methods.